ELEKTROTEHNIŠKI VESTNIK 91(4): 193-202, 2024
ORIGINAL SCIENTIFIC PAPER

An Improved Model Predictive Control for the Virtual Synchronous Generator Based on Modular Multilevel Converters

Haroun Bensiali[1], Farid Khoucha[1], Abdeldjabar Benrabah[1], Mohamed Benbouzid[2]

[1] *Ecole Militaire Polytechnique, UER ELT, Algiers, 16111, Algeria*
[2] *University of Brest, UMR CNRS 6027 IRDL, 29238 Brest, France*
E-mail : d_bensiali.haroun@emp.mdn.dz

Abstract. Modular multilevel converters (MMC) have emerged as a prevalent solution for high- and medium-voltage applications owing to their scalability, modularity, and fault tolerance. However, the associated benefits come hand in hand with the heightened control complexity, particularly when compared to alternative multilevel converter topologies. The paper delves into an advanced control strategy of MMCs for the virtual synchronous generator (VSG) based on the model predictive control (MPC). Within this framework, VSG takes a key role for power management and inertia emulation, aiming to elevate the dynamic response and system stability. Simultaneously, MPC is strategically deployed to optimize the alternating current control, minimize the circulating current, and enhance the direct current control within MMC. The incorporation of the capacitor voltage balancing (CVB) method further plays a crucial role in judiciously redistributing the energy stored in sub-module capacitors, ensuring uniform voltage levels and equalizing the voltage among the capacitors. This comprehensive approach seeks to validate the feasibility and efficacy of the proposed control strategy through detailed simulations and experimental tests. Comparative studies with the PQ-decoupled based control method are conducted to assess the superiority of our strategy in terms of the energy conversion system performance, energy efficiency, and power quality.

Keywords: capacitor voltage balancing method (CVB), modular multilevel converter (MMC), model predictive control (MPC), virtual synchronous generator (VSG), grid-connected MMC.

Napredno krmiljenje navideznega sinhronskega generatorja z modularnimi večnivojskimi pretvorniki

Modularni večnivojski pretvorniki so se pojavili kot prevladujoča rešitev pri visokih in srednjih napetostih zaradi njihove razširljivosti, modularnosti in odpornosti proti napakam. Vendar omenjene koristi spremlja povečana kompleksnost nadzora, zlasti v primerjavi s klasičnimi večnivojskimi pretvorniškimi topologijami. V prispevku je predstavljena napredna strategija krmiljenja navideznega sinhronskega generatorja na osnovi modela prediktivnega nadzora (MPN). MPN optimizira regulacijo električnega toka, zmanjšuje krožni tok, število uporabljenih senzorjev, računsko zahtevnost ter povečuje dinamični odziv. Eksperimentalni testi so potrdili učinkovitost predlaganega pristopa.

Ključne besede: modularni večnivojski pretvornik, modelno napovedno vodenje, navidezni sinhronski generator

1 INTRODUCTION

The continuous growth in the global demand for the renewable energy has elevated the integration of the large-scale renewable energy sources into the power grid to a priority for researchers and engineers around the world [1], [2]. The modular multilevel converter (MMC) is emerging as a promising solution to facilitate the integration, offering a modular and scalable structure that promotes an efficient power conversion and increased grid stability [3], [4], [5].

In the current context of the power systems, MMCs occupy a central position, responding to the challenges posed by the integration of renewable energies and the transmission of the high-voltage direct current (HVDC) [1],[5]. Their scalability means that they can be adapted flexibly to different voltage levels, thus meeting the needs of a variety of applications. The modular design not only simplifies the maintenance, but also offers fault-isolation capabilities and modular expansion potential [6], [7].

Received 23 March 2024
Accepted 21 June 2024

The exceptional resilience of MMCs to component failure enhances their reliability, making them particularly suitable for critical power applications [1], [8]. However, the control complexity associated with MMCs poses a significant challenge. MMCs are renowned for their scalability and modularity, thus so ensuring an effective control while managing the complex multi-tier structure is a considerable challenge [9]. The complexity increases further when it comes to achieving an optimal performance in terms of the power control, reducing unwanted circulating currents, minimizing disturbances on the DC side, as well as balancing the voltages of the SM capacitors [9],[10]. These challenges require innovative control approaches capable of addressing the complexity of MMCs while optimizing their dynamic behavior [11].

One of the key challenges is to strike a delicate balance between the complexity of the control system and its performance [12]. As control strategies become more sophisticated to improve system capabilities, they risk introducing complexities that can hamper the real-time implementation or increase the computational load. Finding the right balance is essential to exploit the full potential of MMCs [8], [13].

The proposed control strategy is designed as a complete solution to the challenges posed by the complexity of the MMC control. It combines the Model Predictive Control (MPC) of the Virtual Synchronous Generator (VSG) and the Capacitor Voltage Balancing (CVB) method to create a synergistic approach for MMCs.

The VSG control component focuses on the power management and inertia emulation, helping to improve the dynamic response and overall stability of the system [14], [15]. By effectively managing power sharing and emulating inertia, VSG improves the MMC ability to respond to dynamic power changes, ensuring an optimal performance under varying operating conditions [16],[17].

MPC is introduced to precisely control the alternating current (AC), reduce the circulating current and improve the direct current (DC) control within MMC. This component ensures an optimal current control, which helps to increase the efficiency and minimize power losses in the converter [18]. The MPC application ensures a precise and adaptive control, contributing to the high-performance objectives of the proposed strategy [19], [20]. The CVB method, a part of the strategy, addresses the challenge of maintaining uniform voltage levels between capacitors within MMC. By using estimation techniques and minimizing switching operations, the CVB method optimizes the converter performance, thus improving the reliability and power quality.

The CVB method is a crucial element in maintaining uniform voltage levels and equalizing voltages between capacitors within SM in MMC. Notable for its sensorless operation, CVB uses estimation techniques, based on mathematical models, to derive capacitor voltages [21]. This sensorless approach improves the control efficiency by reducing the reliance on physical sensors, simplifying the hardware complexity and potentially reducing the overall system costs. In addition, the CVB method aims to strategically minimize the number of switching events in MMC, optimizing the switching schemes to balance the capacitor voltages with a minimum number of events [22], [23]. The reduction in the switching events not only enhances the system reliability but also minimizes the switching losses, leading to an overall improvement in the energy efficiency [24]. To calculate the switching losses of the converter, it is important to know the energy losses at each turn-on and turn-off stage of the insulated gate bipolar transistors (IGBTs) and free-wheeling diodes (FWDs). Consequently, reducing the switching events directly reduces the switching losses [24].

The feasibility analysis extends to a comparative evaluation with the existing methods, including the PQ-CVB control strategy (PQ control combined with the CVB method). The comparative studies provide an insight into the superiority of the proposed strategy in terms of the power conversion system performance. The parameters such as circulating currents, capacitor voltage fluctuations, DC current fluctuation, MMC waveforms and THD are quantitatively evaluated, to understand the advantages of the innovative strategy over the conventional methods.

The rest of the paper is organized as follows Section 2 presents the MMC modeling and operating principle. Section 3 presents the proposed control. Section 4 provides and discusses the simulation and experimental results. Section 5 draws the conclusions of our work.

2 MMC MODELING AND OPERATING PRINCIPLE

Fig. 1(a) shows the structure of three-phase MMC connected to the grid. It consists of three identical phases connected to each other in parallel. Two upper and lower arms (p, n) make up each phase, and each arm is made up of N SMs in series with a L_{arm} inductance and a r_{arm} resistor that demonstrate the power losses in the arm. As shown in Fig. 1(b), each SM is designed with antiparallel IGBTs and diodes, and a capacitor in parallel with each device. SMs in the arm are controlled so that the capacitor is either inserted into the circuit or bypassed. Half-bridge and full-bridge SMs are frequently found as the most commonly used SMs [25], [26].

The MMC inverter is connected to a constant DC current source V_{dc} (V_{dc} represents the output of the MMC rectifier) via a DC line that is modelled by inductance L_{dc} and series resistor r_{dc}. Each MMC phase is connected to the corresponding grid phase by a passive filter comprising inductance L_f and resistor R_f.

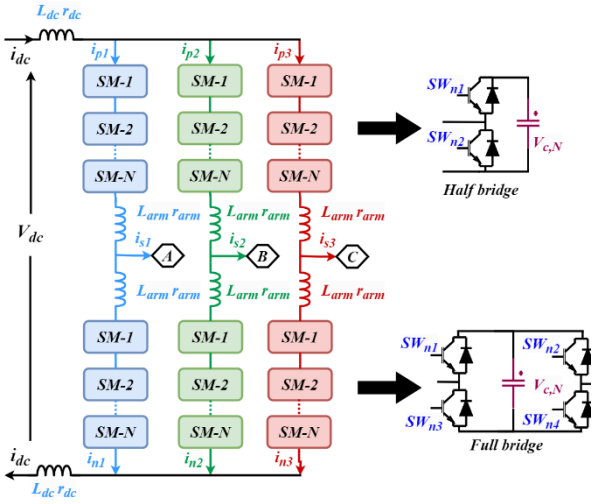

(a) (b)

Figure 1. Multilevel converter topology: (a) equivalent MMC model, (b) SM half bridge and full bridge.

The basic MMC control principle is analyzed based on the dynamics of each converter phase. Applying the Kirchhoff voltage law on an arbitrary phase of Fig. 1(a) gives:

$$i_{x.p} = \frac{i_{x.s}}{2} + \frac{i_{dc}}{3} + i_{x.circ} \tag{1}$$

$$i_{x.n} = -\frac{i_{x.s}}{2} + \frac{i_{dc}}{3} + i_{x.circ} \tag{2}$$

where $i_{x.p}$ and $i_{x.n}$ are the upper and lower arm current, $i_{x.s}$ is the phase current, i_{dc} is the current of the continuous bus, and $i_{x.circ}$ is the circulating current.

$$v_{x.p} = \frac{v_{dc}}{2} - L_{dc}\frac{di_{dc}}{dt} - r_{dc}i_{dc} - L_{arm}\frac{di_{x.p}}{dt} - r_{arm}i_{x.p} - L_f\frac{di_{x.s}}{dt} - R_f i_{x.s} - v_{x.g} \tag{3}$$

$$v_{x.n} = \frac{v_{dc}}{2} - L_{dc}\frac{di_{dc}}{dt} - r_{dc}i_{dc} - L_{arm}\frac{di_{x.n}}{dt} - r_{arm}i_{x.n} + L_f\frac{di_{x.s}}{dt} + R_f i_{x.s} + v_{x.g} \tag{4}$$

where $v_{x.p}$ and $v_{x.n}$ are the upper and lower arm voltage and $v_{x.g}$ is the grid voltage.

Adding (3) and (4) gives the dynamic equation for the DC-bus current:

$$v_{dc} = v_{x.p} + v_{x.n} + 2L_{dc}\frac{di_{dc}}{dt} + 2r_{dc}i_{dc} + L_{arm}\frac{d(i_{x.p} + i_{x.n})}{dt} + r_{arm}(i_{x.p} + i_{x.n}) \tag{5}$$

The DC-bus current is given in terms of the three-phase arm currents:

$$i_{dc} = \sum_{x=a,b,c} i_{x.p} = \sum_{x=a,b,c} i_{x.n} = \frac{1}{2}\sum_{x=a,b,c}(i_{x.p} + i_{x.n}) \tag{6}$$

$$\frac{di_{dc}}{dt} = \frac{1}{6L_{dc} + 2L_{arm}}\left[3v_{dc} - \sum_{x=a,b,c}(v_{x.p} + v_{x.n}) - (6r_{dc} + 2r_{arm})i_{dc}\right] \tag{7}$$

Subtracting (1) and (2) gives the output current:

$$i_{x.s} = i_{x.p} - i_{x.n} \tag{8}$$

Subtracting (3) and (4) gives the dynamic equation for the output current:

$$\frac{di_{x.s}}{dt} = \frac{1}{L_{arm} + 2L_f}\left[v_{x.n} - v_{x.p} - 2v_{x.g} - (r_{arm} + 2R_f)i_{x.s}\right] \tag{9}$$

Adding (1) and (2) gives:

$$i_{x.p} + i_{x.n} = \frac{2}{3}i_{dc} + 2i_{x.circ} \tag{10}$$

Equations (5) and (10) give:

$$v_{dc} = v_{x.p} + v_{x.n} + (2L_{dc} + \frac{2}{3}L_{arm})\frac{di_{dc}}{dt} + (2r_{dc} + \frac{2}{3}r_{arm})\,i_{dc} + 2L_{arm}\frac{di_{x.circ}}{dt} + 2r_{arm}i_{x.circ} \tag{11}$$

Equations (7) and (11) provide the dynamic model of the below circulating current:

$$\frac{di_{x.circ}}{dt} = \frac{1}{6L_{arm}}\left[\sum_{x=a,b,c}(v_{x.p} + v_{x.n}) - 3(v_{x.p} + v_{x.n}) - 6r_{arm}i_{x.circ}\right] \tag{12}$$

3 THE PROPOSED CONTROL SYSTEM

The proposed control method combines the MPC control of VSG with the CVB capacitor voltage balancing to improve the MMC system control performance. The VSG control facilitates power sharing, improves the system dynamic response, inertia emulation and system stability. The MPC control simultaneously controls the AC-side currents, eliminates/minimizes the circulating currents and controls the DC-side current by eliminating/minimizing the disturbance. The CVB method is used to redistribute the energy stored in the SMs capacitors, thus ensuring uniform voltage levels, equalizing the voltage between the capacitors and minimizing SMs switching to reduce switching losses. The proposed control design for the grid-connected MMC is illustrated in Fig. 2.

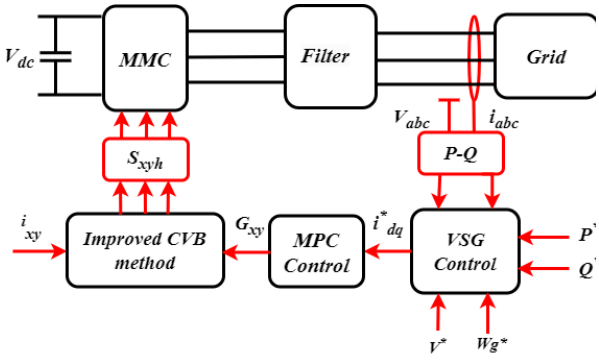

Figure 2. Block diagram of the proposed CVB-VSG control.

3.1 VSG-based control

The VSG-based control is used to simulate the behavior of a synchronous generator in a grid-connected MMC system. It controls the active and reactive power [14], [15]. The VSG control scheme is shown in Fig. 3.

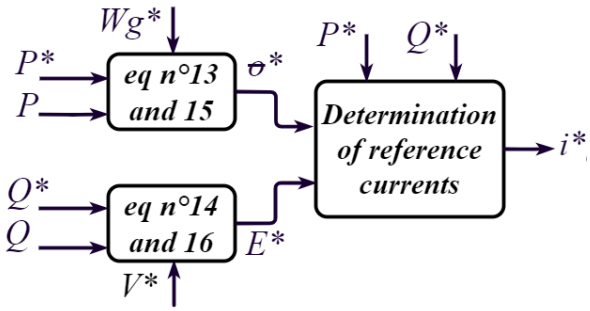

Figure 3. VSG-based control scheme.

The frequency and voltage drop characteristics introduced by the VSG control are typical of the synchronous generators. It enables MMC to offer a frequency control and inertial response similar to that of the traditional synchronous generators. The voltage drop control allows MMC to adapt its output power to variations in the mains frequency and voltage. This behavior keeps the grid stable and inert [16], [17].

The VSG mathematical model is based on the second-order model of a synchronous generator, as well as the mechanical rotor rotation and stator voltage equations [17].

$$J\frac{d\omega}{dt} = \frac{P_m - P_e}{\omega} - D(\omega - \omega_g) \quad (13)$$

$$e_{abc} = v_{abc} - Ri_{abc} - L\frac{di_{abc}}{dt} \quad (14)$$

where P_m is the mechanical power, P_e is the electromagnetic power, J and D are the inertia and damping, respectively, ω is the rotor angular frequency, ω_g is the actual angular frequency of the grid, e_{abc}, v_{abc} and i_{abc} are the excitation voltage, terminal voltage and stator current of SG, respectively. R is the armature resistance and L is the synchronous reactance.

The VSG drop control mathematical model to control the frequency and voltage is expressed as:

$$\omega_g = \omega_N + D_P(P_N - P) \quad (15)$$

$$U = U_N + D_q(Q_N - Q) \quad (16)$$

where P_N and Q_N are the rated active power and reactive power, respectively. P and Q are the VSG active and reactive power, respectively. D_P is the P-ω drop coefficient and D_q is the Q-U drop coefficient. U_N is the rated voltage amplitude. ω_N is the rated angular frequency.

3.2 MPC control

The functional diagram of the MPC approach is shown in Fig. 4. The methodology requires a discrete-time model of the MMC system. The MPC objective is to simultaneously control the output currents, eliminate/minimize the circulating currents, and control the DC-side current.

The proposed MPC strategy is based on the following steps:

- Development of a discrete-time model for a one-step prediction of the control variables.
- Definition of the cost function g incorporating the control objectives and constraints.
- Evaluation of the defined cost function for all possible inserted SM numbers G_{xy}.
- Selection of best possible numbers G_{xy} to minimize the cost function g_{min}.

The MPC implementation requires the conversion of the continuous-time MMC model into a discrete-time model. Various discretization methods can be applied [19], primarily based on a numerical integration or differentiation techniques.

The MMC dynamic model presented in Section 2 is composed of ordinary differential equations that can be solved using various approximation methods, especially the Euler method. The latter is widely preferred in the field of power electronic systems due to its simplicity, direct implementation, and low computational burden [19], [20].

Considering the first-order differential equation:

$$\frac{dx(t)}{dt} = \mathrm{u(t)} \quad (17)$$

The Euler approximation is given by

$$\left\{\frac{dx(t)}{dt}\right\}_{t=KT_s} \approx \frac{x(KT_s + T_s) - x(KT_s)}{T_s} \quad (18)$$

$$x(KT_s + T_s) \approx x(KT_s) + T_s\left\{\frac{dx(t)}{dt}\right\}_{t=KT_s} \quad (19)$$

$$x(KT_s + T_s) \approx x(KT_s) + T_s u(KT_s) \quad (20)$$

Equation 16 shows that the future evolution of control variable $x(k+1)$ is conditioned by its current state $x(k)$ as well as the current value of the input variable $u(k)$. By leveraging the equation, it becomes possible to anticipate and calculate the future state of the control variable based on these two affecting parameters.

Using the Euler approach and with equations (7), (9) and (12), the derivatives of the DC bus current, the output current and the circulating current, respectively, can be approximated as follows:

$$i_{dc}^{P}(K+1) = \alpha i_{dc}^{m}(K) + \beta\left[3v_{dc}^{m}(K) - \sum_{x=a,b,c}(v_{x.p}^{P}(K) + v_{x.n}^{P}(K))\right] \quad (21)$$

where $\alpha = 1 - \frac{(6r_{dc}+2r_{arm})T_s}{6L_{dc}+2L_{arm}}$; $\beta = \frac{T_s}{6L_{dc}+2L_{arm}}$

$$i_{x.s}^{P}(K+1) = \gamma\, i_{x.s}^{m}(K) + \delta\left[v_{x.n}^{P}(K) - v_{x.p}^{P}(K) - 2v_{x.g}^{m}(K)\right] \quad (22)$$

where $\gamma = 1 - \frac{(r_{arm}+2R_f)T_s}{L_{arm}+2L_f}$; $\delta = \frac{T_s}{L_{arm}+2L_f}$

$$i_{x.circ}^{P}(K+1) = \rho\, i_{x.circ}^{m}(K) + \sigma\left[\sum_{x=a,b,c}(v_{x.p}^{P}(K) + v_{x.n}^{P}(K)) - 3\left(v_{x.p}^{P}(K) + v_{x.n}^{P}(K)\right)\right] \quad (23)$$

where $\rho = 1 - \frac{r_{arm}T_s}{L_{arm}}$; $\sigma = \frac{T_s}{6L_{arm}}$

The main cost function aggregates various control variables. Each is assigned a weighting coefficient according to the priority assigned to the control objective [19]. The expression of the cost function is:

$$g = \lambda 1|i_{x.s}^{*} - i_{x.s}^{P}| + \lambda 2\left|i_{dc}^{*} - i_{dc}^{P}\right| + \lambda 3\left|i_{x.circ}^{*} - i_{x.circ}^{P}\right| \quad (24)$$

Weighting factors *λ1*, *λ2* and *λ3* are the most important parameters adjusting the priority between the control objectives. Their significant impact on the control behavior and stability emphasizes the importance of their judicious selection [19].

In the process of selecting the vector of the numbers for active submodules G_{xy}, the approach involves choosing the vector that minimizes the cost function. This optimal vector is then applied in the subsequent sampling period, contributing to a continuous optimization of the control.

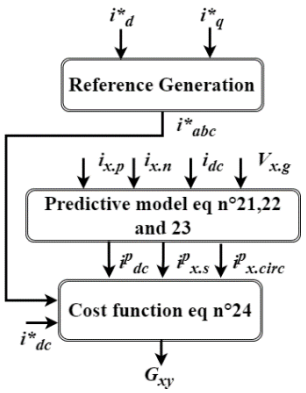

Figure 4. Block diagram of the MPC control.

3.3 Improved CVB method

The proposed CVB method plays a vital role in the reliable operation MMC. The method relies on controlling the charging and discharging of the SM capacitors based on the direction of the arm current and the instantaneous capacitor voltage using a logic function-based algorithm [22], [23] shown in Fig. 5.

The proposed CVB method offers several advantages, such as scalability and straightforward programming. It eliminates the need for a *PI* controller to set capacitor voltages. Instead it utilizes an algorithm based on a simple logic comparison.

In order to implement the CBV method, the SM capacitor voltages in each arm are estimated using the dynamic equation of the SM capacitor voltage:

$$i_{cxyn} = C\frac{dV_{cyn}}{dt} \quad (25)$$

where i_{cxyn} and V_{cyn} are the SM current and SM capacitor voltage, respectively. x is the phase (x=a, b, c) and y represents the arm (y=p, n).

Using the Euler approximation and assuming the sampling period of T_s, the predicted SM capacitor voltages at a discrete time are derived from equation (26):

$$V_{cyn}(t+T_s) = V_{cyn}(t) + i_{xy}\frac{T_s}{C} \quad (26)$$

where i_{xy} is the upper or lower arm current.

The estimated SM capacitor voltages are introduced into the comparison logic to compare each capacitor voltage to obtain index number *Ih*. The highest index number corresponds to the lowest capacitor voltage and vice versa. Arm current direction *d* is then determined.

SMs are then sorted in an ascending or descending order of the SM index numbers according to the direction of the arm current using equation (27) which presents actual index number *Ah*:

$$Ah = Ih \times d + (N - 1 - Ih) \times (1 - d) \quad (27)$$

SMs with the lowest capacitor voltage are inserted for the positive current direction and are charged. Similarly, SMs with the highest capacitor voltage are inserted for the negative current direction and are discharged.

The required number of inserted SMs G_{xy} is obtained from output vector generation command MPC. Insertion and bypass (short-circuit) states M_{xyh} for each SM are generated by comparing actual index number *Ah* with reference index number N-G_{xy}.

Finally, the calculations optimization is performed by comparing the inserted SMs G_{xy} current number with the inserted SMs $G^{p}{}_{xy}$ previous number.

If the voltage levels are different, the algorithm applies new control signals (i.e., $S_{xyh} = M_{xyh}$). Otherwise, the algorithm maintains the previous switching state (i.e., $S_{xyh} = M^{p}{}_{xyh}$).

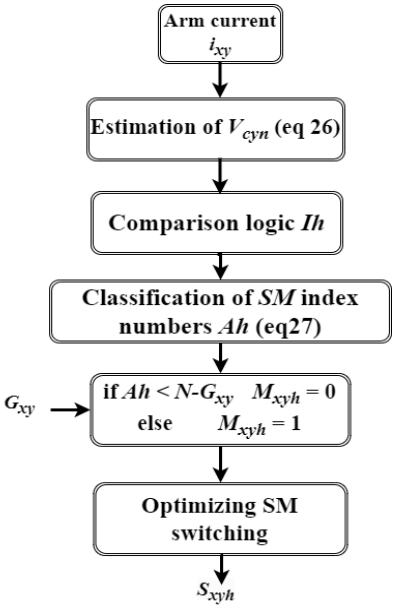

Figure 5. Block diagram of the MPC control.

4 SIMULATION AND EXPERIMENTAL RESULTS

4.1 Simulation results

To evaluate the effectiveness of the proposed VSG-MPC-CVB control, numerical simulations are carried out in the MATLAB/Simulink environment. The results are compared with the conventional PQ-decoupled control using the CVB method. The parameters shown in Table 1 are used for each simulation.

Table 1. Electric power system parameters

	Value	
Parameters	**Simulation**	**Experimental**
DC Voltage (VDC)	800 V	100 V
AC Voltage (VAC)	220 V	30 V
AC frequency	50 Hz	50 Hz
Number of SMs per arm	2	2
Capacitor value for SM	50 mF	3.3 mF
Arm inductance / Arm resistor	1 mH/ 0.5Ω	10 mH/ 0.5Ω
Phase inductor / Phase resistor	20 mH/ 0.5Ω	20 mH/ 0.5Ω

Different situations of the active power-injected variation are analyzed to evaluate the tracking behavior of the proposed VSG-MPC-CVB control. In the first case, the injected constant active power is 7 KW from 0 to 0.5 s. The active power increases from 7 to 9 kW between 0.5 and 1 s. The active power remains constant at 9 KW between 1 and 1.5 s.

Fig. 6 shows the simulation results for the two control strategies used in MMC, i.e. the PQ-CVB and VSG-MPC-CVB control.

Figs. 6(a) and 6(b) show the steady-state current and voltage waveforms of MMC and the grid, respectively. The MMC voltages are balanced and consist of five identical levels (2N+1). The 50 Hz currents are sinusoidal. The estimated capacitor voltages of phase A SMs are shown in Figs. 6(c) and 6(d) for the PQ-CVB and VSG-MPC-CVB controls, respectively. The SM voltage fluctuation range is 0.25 V for PQ-CVB and 0.15 V for VSG-MPC-CVB.

When there is a change in the power injected into the grid, the SM capacitor voltages deviate to adjust to the steady state (see Fig. 6(e)). The SM voltage fluctuations in the same arm are identical and complementary between the upper and lower arms. The difference between the SM voltage and the reference voltage (200 V) is 1.75 V for the PQ-CVB control and 0.1 V for the VSG-MPC-CVB control.

The total harmonic distortion (THD) of the alternating currents is low in the VSG-MPC-CVB control. It is 0.07% compared to 0.37% of the PQ-CVB control (see Fig. 6(f)).

The circulating currents of the CVB-PQ and VSG-MPC-CVB control are shown in Figs. 6(g) and 6(h) below, respectively. The fluctuation of the circulating current is from -3.8 A to 3.8 A for the PQ-CVB control and from -0.2 A to 0.2 A for the VSG-MPC-CVB control. Figs. 6(g) and 6(h) above show that the DC current is more stable for the VSG-MPC-CVB control than for the PQ-CVB control. It can be seen that the DC current fluctuations for the VSG-MPC-CVB control are zero, and the CVB-PQ control fluctuates by 0.5A.

Fig. 6(i) shows that the active and reactive power follow the power references. However, an important observation is that the response time of the VSG-MPC-CVB command is significantly shorter than that of the PQ-CVB command when changing the power reference.

Table 2 shows numerical simulation results, utilizing relevant measures and indicators to evaluate the performance of the PQ-CVB and VSG-MPC-CVB control methods. The presentation is a valuable tool enabling a precise analysis and enhancing understanding of the effectiveness of the two control methods.

The incorporation of the performance measures in Table 2 allows a systematic comparison to identify the advantages and disadvantages of each control method. Such quantitative evaluation streamlines the decision-making process, supporting the selection and implementation of control strategies in the relevant applications.

Table *2.* Numerical Results simulation for the PQ-CVB and VSG-MPC-CVB Control.

Control	THD	ΔIdc	ΔIcirc	ΔVc	$Vc_{ref} - Vc_{estm}$
PQ-CVB	0.37%	0.5A	6.8A	0.25V	1.75 V
VSG-MPC-CVB	0.07%	0A	0.4A	0.15V	0.1 V

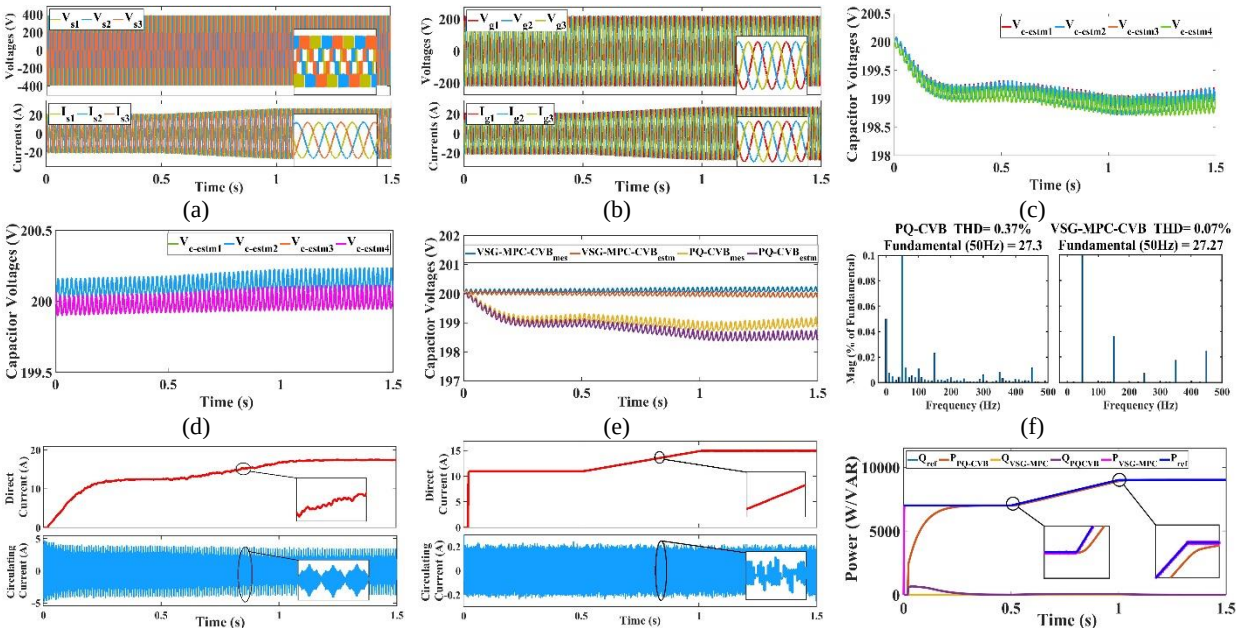

Figure 6. Simulation results of applying the VSG-MPC-CVB and PQ-CVB control to MMC. (a) The MMC three-phase voltages and currents. (b) Three-phase voltages and currents of the grid. (c) Estimation of the voltages of the SMs capacitor of phase A using the PQ-CVB control. (d) Estimation of the voltages of the SMs capacitor of phase A using the VSG-MPC-CVB control. (e) Estimation and measurement of phase A SM capacitor voltages for both commands. (f) THD of MMC current Phase A. (g) Average value of the DC current (above) and circulating current (below) for the PQ-CVB control. (h) Average value of the DC current (above) and circulating current (below) for the VSG-MPC-CVB control. (i) Active and reactive power.

4.2 Experimental results

To assess the effectiveness of the proposed control strategy, an experimental prototype of a reduced-scale three-phase MMC Converter is set up in our laboratory (see Fig. 7). Experimental parameters are listed in Table 1. The MMC Control is made based on our research and control board "*μ-tech*."

Three variations of the active power are applied to test the control strategy. A constant power of 95 W from 0 to 60 s is maintained. It is followed by an increase to 120 W from 60 to 100 s. It is then stabilized at 120 W until 120 s. The experimental results of the two control strategies applied to MMC are graphically presented in Fig. 8.

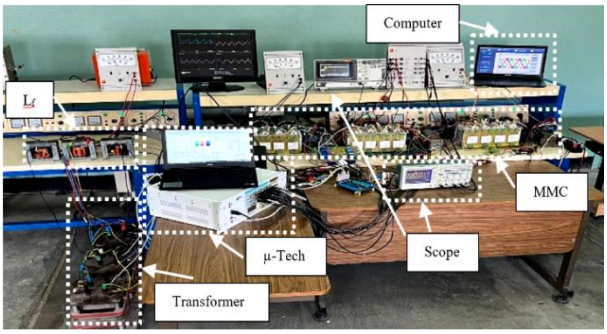

Figure 7. Experimental platform of the three-phase MMC.

Fig. 8(a) depicts the steady-state waveforms of the MMC output voltage. It is shown that the waveform exhibits on enhanced characteristic when employing the proposed control strategies, where five balanced and stable levels are observed. In contrast, the PQ-CVB strategy results in unstable and unbalanced voltage levels, leading to a disappearance of the internal levels.

Fig. 8(b) shows the currents and voltages of the grid in its steady state. The voltage waveform is sinusoidal and the current is constant at 1.4 A from 0 to 60 s. It is followed by an increase to 1.7 A from 60 to 100 s. It then stabilizes at 1.7 A until 120 s, corresponding to the power reference levels. When comparing the PQ-CVB and VSG-MPC-CVB control strategy, it is evident that the former exhibits improved current waveforms with fewer fluctuations.

The SM capacitor voltages in phase B are depicted in Fig. 8(c) for the control strategies PQ-CVB and VSG-MPC-CVB. In the event of variations in the injected active power, the voltages of the SM capacitors remain stable, balanced, and equal to the reference voltage (Vdc/N), which is set at 50V. The fluctuation range of the SM voltages is between 49.5 V and 50.5 V for the VSG-MPC-CVB control and between 48.5 V and 51.5 V for the PQ-CVB control.

The circulating currents of the PQ-CVB and VSG-MPC-CVB controls are illustrated in Fig. 8(d). The circulating current is minimal with lower fluctuations when utilizing the proposed control, ranging from -0.5 A to 0.5 A, compared to the PQ-CVB control, which varies between -0.9 A and 0.9 A.

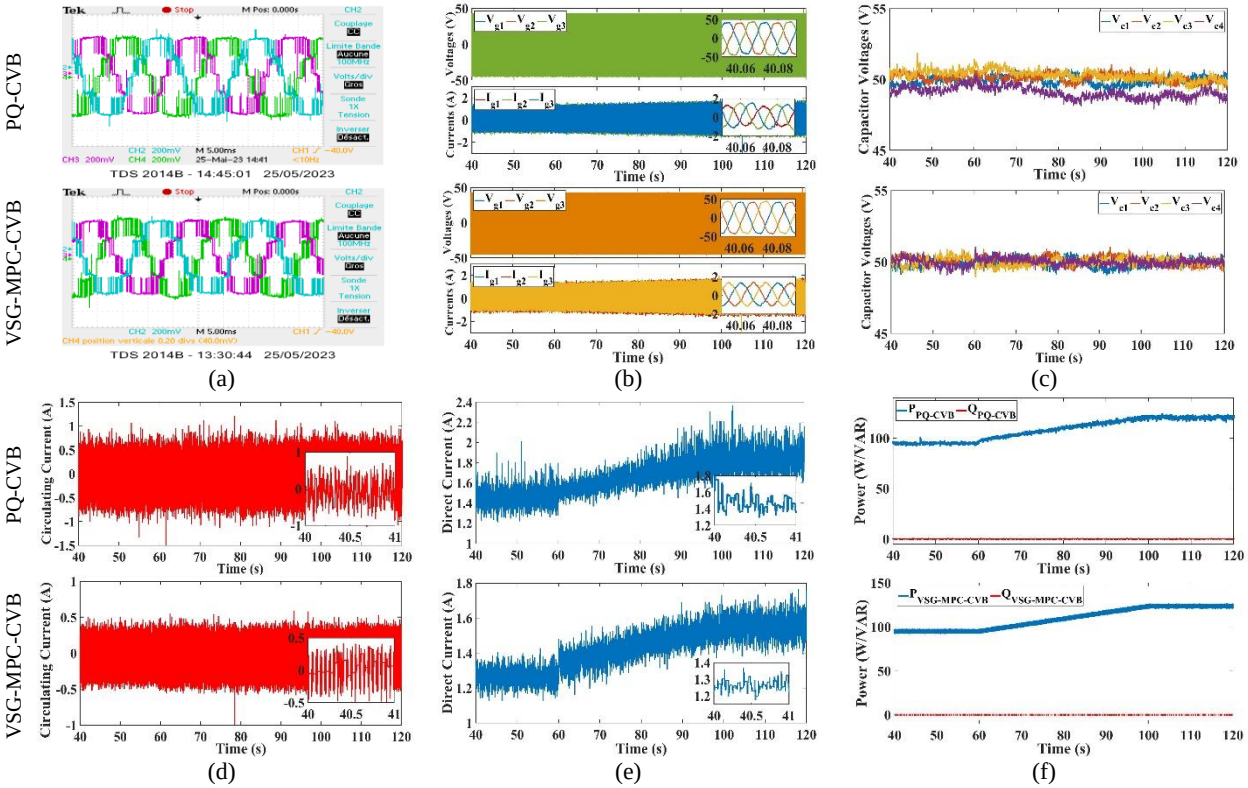

Figure 7. Experimental results of applying the VSG-MPC-CVB and PQ-CVB control to MMC. (a) Three-phase voltages of MMC. (b) Three-phase voltages and currents of the grid. (c) Voltages of the SM capacitors in phase B. (d) Phase A circulating current. (e) DC current. (f) Active and reactive power.

Fig. 8(e) illustrate the DC current for the PQ-CVB and VSG-MPC-CVB controls. The DC current is more stable with lower fluctuations (0.2A) in the VSG-MPC-CVB control compared to the PQ-CVB control (fluctuations of 0.5A).

Fig. 8(f) shows that the active and reactive power follow the power references (0 VAR for the reactive power) for the control strategies PQ-CVB and VSG-MPC-CVB. A slight disturbance in the active power (P=120 W) is observed for the PQ-CVB control. The VSG-MPC-CVB control exhibits a greater stability.

The numerical data in Table 3 obtained from our practical validation, serves as a robust basis for the evaluation and comparison of the two control method. The practical validation offers a real-world insight into the performance of each method, allowing for a comprehensive analysis of their effectiveness.

Table *2*.Numerical Data from a Practical validation for the PQ-CVB and VSG-MPC-CVB control.

Control	ΔIdc	ΔIcirc	ΔVc	$Vc_{ref} - Vc_{estm}$
PQ-CVB	0.5A	1.8A	1 V	1.5 V
VSG-MPC-CVB	0.2A	1A	3 V	0.5 V

The obtained results underscore the efficiency of the SM capacitor voltage balancing techniques, particularly the CVB strategy, as a compelling solution for enhancing the stability and performance of the MMC systems.

5 Conclusion

A new VSG-MPC-CVB control system is proposed to control the grid-connected MMC systems. The control method integrates the MPC control with the CVB balancing technique. The proposed control incorporates VSG for power sharing and inertia emulation to improve the dynamic response and stability of the system. The MPC controller cost function is designed to improve the grid current control, minimize the circulating current and improve the MMC DC control. The simplified CVB method is used to estimate the capacitor voltage and to optimize the switching frequency.

The performed simulations and experimental tests validate the effectiveness of the proposed control strategy by comparing it with the PQ-CVB control. The results highlight the suitability of VSG-MPC-CVB to control grid-connected MMC-based systems. The proposed control technique also minimizes the circulating current, reduces the DC-side disturbances, eliminates the need for an extensive sensor deployment, reduces computational requirements and allows for a faster dynamic response.

References

[1] Kumar, G. B., Sarojini, R. K., Palanisamy, K., Padmanaban, S., & Holm-Nielsen, J. B. “Large scale

renewable energy integration: Issues and solutions". Energies, 12(10), pp. 1996, 2019
https://doi.org/10.3390/en12101996

[2] Yang, S., Fang, J., Tang, Y., Qiu, H., Dong, C., & Wang, P. "Modular multilevel converter synthetic inertia-based frequency support for medium-voltage microgrids". IEEE Transactions on Industrial Electronics, 66(11), pp. 8992-9002, 2019.
https:// 10.1109/TIE.2018.2890491

[3] Shahnazian, F., Adabi, J., Pouresmaeil, E., & Catalão, J. P. "Interfacing modular multilevel converters for grid integration of renewable energy sources". Electric Power Systems Research, 160, pp. 439-449, 2018.
https://doi.org/10.1016/j.epsr.2018.03.014

[4] Wang, W., Li, G., & Guo, J. "Large-scale renewable energy transmission by HVDC: Challenges and proposals". Engineering, 19, pp. 252-267, 2022.
https://doi.org/10.1016/j.eng.2022.04.017

[5] Mahmoud, A. A., Hafez, A. A., & Yousef, A. M. "Modular multilevel converters for renewable energies interfacing: Comparative review". In 2019 IEEE Conference on Power Electronics and Renewable Energy (CPERE), pp. 397-406, 2019.
https://10.1109/CPERE45374.2019.8980038

[6] Liu, X., Li, G., Zheng, T., Yang, X., & Guerrero, J. M. "Thyristor-pair-and damping-submodule-based protection against valve-side single-phase-to-ground faults in MMC-MTDC systems". IEEE Transactions on Power Delivery, 37(4), pp. 3257-3269, 2021.
https://10.1109/TPWRD.2021.3125661

[7] Soomro, J. B., Akhtar, F., Hussain, R., Ahmed Ansari, J., & Munir, H. M. "A detailed review of MMC circuit topologies and modelling issues". International Transactions on Electrical Energy Systems, 2022.
https://doi.org/10.1155/2022/8734010

[8] Perez, M. A., Ceballos, S., Konstantinou, G., Pou, J., & Aguilera, R. P. « Modular multilevel converters: Recent achievements and challenges". IEEE Open Journal of the Industrial Electronics Society, 2, pp. 224-239, 2021.
https:// 10.1109/OJIES.2021.3060791

[9] Cui, T., Wang, W., & Wang, H. "MMC-HVDC High-Frequency Resonance Suppression Strategy Based on Multi-Band Band-Stop Filters". Sustainability, 15(18), pp. 13309, 2023.
https://doi.org/10.3390/su151813309

[10] Wang, Y., Liao, S., Xu, Q., Wang, L., & Guerrero, J. M. "Coordinated design of control parameters for improving interactive and internal stability of MMC-HVDC". International Journal of Electrical Power & Energy Systems, 140, pp. 108065, 2022.
https://doi.org/10.1016/j.ijepes.2022.108065

[11] Atanalian, S., Sebaaly, F., Arazm, S., Zgheib, R., Al-Haddad, K., & Kanaan, H. Y. "Three-phase ZPUC-MMC grid connected converter". In IECON 2022–48th Annual Conference of the IEEE Industrial Electronics Society, pp. 1-6, 2022.
https://10.1109/IECON49645.2022.9968917

[12] Vozikis, D., Alsokhiry, F., & Adam, G. P. "Analysis and experimental verification of improved two-level converter behaviors under unbalanced AC conditions". International Journal of Electrical Power & Energy Systems, 133, pp. 107266, 2021.
https://doi.org/10.1016/j.ijepes.2021.107266

[13] HosseinNataj, S., Gholamian, S. A., Rezanejad, M., & Mehrasa, M. "Virtual synchronous generator-based control of modular multilevel converter for integration into weak grid". IET Renewable Power Generation, 17(12), pp. 3097-3107, 2023.
https://doi.org/10.1049/rpg2.12828

[14] Belila, A., Amirat, Y., Benbouzid, M., Berkouk, E. M., & Yao, G. "Virtual synchronous generators for voltage synchronization of a hybrid PV-diesel power system". International Journal of Electrical Power & Energy Systems, 117, pp. 105677, 2020.
https://doi.org/10.1016/j.ijepes.2019.105677

[15] Li, Z., Li, H., Zheng, X., & Gao, M. "Virtual model predictive control for virtual synchronous generators to achieve coordinated voltage unbalance compensation in islanded micro grids". International Journal of Electrical Power & Energy Systems, 146, pp.108756, 2023.
https://doi.org/10.1016/j.ijepes.2022.108756

[16] Ali, H., Li, B., Xu, Z., Liu, H., & Xu, D. "Virtual synchronous generator design based modular multilevel converter for microgrid frequency regulation". In 2019 22nd International Conference on Electrical Machines and Systems (ICEMS), pp. 1-6, 2019.
https://10.1109/ICEMS.2019.8921603

[17] Babayomi, O., Zhang, Z., Dragicevic, T., Hu, J., & Rodriguez, J. "Smart grid evolution: Predictive control of distributed energy resources—A review". International Journal of Electrical Power & Energy Systems, 147, pp. 108812, 2023.
https://doi.org/10.1016/j.ijepes.2022.108812

[18] Harbi, I., Rodriguez, J., Liegmann, E., Makhamreh, H., Heldwein, M. L., Novak, M., & Kennel, R. "Model Predictive Control of Multilevel Inverters: Challenges, Recent Advances, and Trends". IEEE Transactions on Power Electronics, 2023.
https://10.1109/TPEL.2023.3288499

[19] Akbari, E., & Shadlu, M. S. "Model Predictive Control of Alternate Arm Converter with a Short-Overlap Period Under Steady-State and Transient Conditions". In 2023 14th Power Electronics, Drive Systems, and Technologies Conference (PEDSTC), pp. 1-7, 2023.
https://10.1109/PEDSTC57673.2023.10087124

[20] Gobburi, H. B., Borghate, V. B., & Meshram, P. M. "Voltage Balancing method for Modular Multilevel Converter with Sensorless Operation". In 2022 IEEE IAS Global Conference on Emerging Technologies (GlobConET), pp. 828-833, 2022.
https:// 10.1109/GlobConET53749.2022.9872328

[21] Dekka, A., Wu, B., Zargari, N. R., & Fuentes, R. L. "Dynamic voltage balancing algorithm for modular multilevel converter: A unique solution". IEEE Transactions on power electronics, 31(2), pp. 952-963, 2015. https:// 10.1109/TPEL.2015.2419881

[22] Al-Khayyat, A. S., Ridha, A. A., & Fadel, H. "Performance analysis of capacitor voltage balancing in modular multilevel converter by sorting algorithm". International Journal of Power Electronics and Drive Systems, 13(3), pp. 1548, 2022. http://doi.org/10.11591/ijpeds.v13.i3.pp1548-1557

[23] Zhu, Y., Xiao, M., Su, X., Yang, G., Lu, K., & Wu, Z. "Modeling of conduction and switching losses for IGBT and FWD based on SVPWM in automobile electric drives". Applied Sciences, 10(13), pp. 4539, 2020. https://doi.org/10.3390/app10134539

[24] Wang, C., Xu, J., Pan, X., Gong, W., Zhu, Z., & Xu, S. "Impedance modeling and analysis of series-connected modular multilevel converter (MMC) and its comparative study with conventional MMC for HVDC applications". IEEE Transactions on Power Delivery, 37(4), pp. 3270-3281, 2021. https://10.1109/TPWRD.2021.3125699

[25] Bensiali, H., Khoucha, F., Benrabah, A., Belila, A., & Benbouzid, M. "Comparative Analysis of Modular Multilevel Converters and Alternate Arm Converters for HVDC Applications". In Artificial Intelligence and Heuristics for Smart Energy Efficiency in Smart Cities: Case Study: Tipasa, Algeria (pp. 312-321). Springer International Publishing, 2022. https://doi.org/10.1007/978-3-030-92038-8_32

[26] Liu, X., Sun, P., Arraño-Vargas, F., & Konstantinou, G. "Provision of synthetic inertia by alternate arm converters in VSC-HVDC systems". In 2021 31st Australasian Universities Power Engineering Conference (AUPEC), pp. 1-5, 2021. https:// 10.1109/AUPEC52110.2021.9597753

Haroun Bensiali received his engineering degree in electrical engineering from the Ecole Militaire Polytechnique, Algiers, Algeria, in 2018. He is currently working towards his Ph.D. degree at the same institution and in collaboration with the University of Brest, Brest, France.

His research interests include control of grid-connected converters, renewable energy, HVDC systems, and multilevel converter.

Farid Khoucha received his Ph.D. degree in electrical engineering from the Ecole Militaire Polytechnique, Alger, Algeria, in 2012. In 2000, he joined the same institution as a Teaching Assistant. Since January 2013, he has been Associate Professor.

His current research interests include electric and hybrid vehicle control and energy management, renewable energy, smart grids, MVDC and HVDC systems, and modular multilevel converter.

Abdeldjabar Benrabah received his engineering degree in electrical engineering from the Ecole Militaire Polytechnique, Alger, Algeria, in 2012, and his Ph.D. degree in electrical engineering from the Harbin Institute of Technology, Harbin, China, in 2018. He is currently an Associate Professor with the Electrical Engineering Department of the Ecole Militaire Polytechnique, Algeria. In 2017, he was a recipient of the Chinese Government Outstanding International Student Scholarship.

His research interests include power conversion control, renewable energy and micro-grids.

Mohamed Benbouzid received his Ph.D. degree in electrical engineering from the National Polytechnic Institute of Grenoble, Grenoble, France, in 1994. In 2000, he was granted a Habilitation as a Researcher from the University of Amiens, Amiens, France.

Since 2004 he has been holding the position of an Associate Professor in electrical engineering and since 2004 he has been affiliated with the University of Brest, France, where he is currently working as a Full Professor in the field of electrical engineering. He also holds the position of a Distinguished Professor and is a 1000 Talent Expert at the Shanghai Maritime University, China. He is an IEEE and IET Fellow. He is the Editor-in-Chief of the International Journal on Energy Conversion and the Applied Sciences (MDPI) Section on Electrical, Electronics and Communications Engineering. He is a Subject Editor for the IET Renewable Power Generation.

His main research interests and expertise include control of electric machines, variable-speed drives for traction, propulsion, and renewable energy applications, and fault diagnosis of electric machines.